

# Physico-chemical characterization of SOA derived from catechol and guaiacol – a model substance for the aromatic fraction of atmospheric HULIS

J. Ofner<sup>1</sup>, H.-U. Krüger<sup>1</sup>, H. Grothe<sup>2</sup>, P. Schmitt-Kopplin<sup>3,5</sup>, K. Whitmore<sup>4</sup>, and C. Zetzsch<sup>1</sup>

<sup>1</sup>Atmospheric Chemistry Research Laboratory, University of Bayreuth, Germany

<sup>2</sup>Institute of Materials Chemistry, Vienna University of Technology, Austria

<sup>3</sup>Institute of Ecological Chemistry, Helmholtz Zentrum Munich, Germany

<sup>4</sup>University Service Centre for Transmission Electron Microscopy, Vienna University of Technology, Austria

<sup>5</sup>Department for Chemical-Technical Analysis, Research Center Weihenstephan for Brewing and Food Quality, Technical University Munich, Freising-Weihenstephan, Germany

Received: 28 June 2010 – Published in Atmos. Chem. Phys. Discuss.: 20 July 2010

Revised: 4 December 2010 – Accepted: 7 December 2010 – Published: 3 January 2011

**Abstract.** Secondary organic aerosol (SOA) was produced from the aromatic precursors catechol and guaiacol by reaction with ozone in the presence and absence of simulated sunlight and humidity and investigated for its properties as a proxy for HUmic-Like Substances (HULIS). Beside a small particle size, a relatively low molecular weight and typical optical features in the UV/VIS spectral range, HULIS contain a typical aromatic and/or olefinic chemical structure and highly oxidized functional groups within a high chemical diversity. Various methods were used to characterize the secondary organic aerosols obtained: Fourier transform infrared spectroscopy (FTIR) demonstrated the formation of several carbonyl containing functional groups as well as structural and functional differences between aerosols formed at different environmental conditions. UV/VIS spectroscopy of filter samples showed that the particulate matter absorbs far into the visible range up to more than 500 nm. Ultrahigh resolved mass spectroscopy (ICR-FT/MS) determined O/C-ratios between 0.3 and 1 and observed  $m/z$  ratios between 200 and 450 to be most abundant. Temperature-programmed-pyrolysis mass spectroscopy (TPP-MS) identified carboxylic acids and lactones/esters as major functional groups. Particle sizing using a condensation-nucleus-counter and differential-mobility-particle-sizer (CNC/DMPS) monitored the formation of small particles during the SOA formation process.

Particle imaging, using field-emission-gun scanning electron microscopy (FEG-SEM), showed spherical particles, forming clusters and chains. We conclude that catechol and guaiacol are appropriate precursors for studies of the processing of aromatic SOA with atmospheric HULIS properties on the laboratory scale.

## 1 Introduction

Atmospheric aerosol particles strongly influence the global atmosphere, and their contribution to climate change is versatile (Forster et al., 2007). Especially SOA play a major role in the impact of atmospheric chemistry on climate. Mass fluxes of 30–270 Tg yr<sup>-1</sup> have been estimated to be emitted per year by tropospheric oxidation of biogenic and anthropogenic volatile organic compounds (Andreae and Crutzen, 1997). Contributions to the fine aerosol of organic materials between 20–50% at mid-latitudes and up to 90% in tropical forested areas are reported and reviewed by Kanakidou et al. (2005). According to aromatic SOA precursors they report anthropogenic emissions of 6.7 Tg yr<sup>-1</sup> toluene, 4.5 Tg yr<sup>-1</sup> xylene, 0.8 Tg yr<sup>-1</sup> trimethylbenzene, and 3.8 Tg yr<sup>-1</sup> of other aromatic compounds. Hallquist et al. (2009) report total biogenic SOA fluxes of 12–70 Tg yr<sup>-1</sup> from bottom-up estimates. Fluxes of 17 TgC yr<sup>-1</sup> for SOA from biomass burning and 10 TgC yr<sup>-1</sup> for SOA from



Correspondence to: H. Grothe  
(grothe@tuwien.ac.at)

anthropogenic sources are reported by them based on a top-down approach.

While the formation of SOA from different terpenes (e.g. Jonsson et al., 2007; Jonsson et al., 2008; Iinuma et al., 2004) has been studied in detail and summarized in recent reviews (Yu et al., 2008; Kroll and Seinfeld, 2008), there is still a lack of knowledge of SOA formation from aromatic precursors (Johnson et al., 2005). The atmospheric oxidation of benzene has been studied in detail (e.g. Lay et al., 1996). Forstner et al. (1997) studied the formation of SOA from toluene- and xylene-type precursors, discussing ring-opening mechanisms based on reactions with hydroxyl radicals. Studies on formation and processing of those precursors according to SOA formation at  $\text{NO}_x$  conditions have been performed by Ng et al. (2007) and Jang and Kamens (2001). Fisseha et al. (2004) used 1,3,5-trimethylbenzene as precursor and determined a contribution of 20–45% of organic acids to the overall aerosol mass. Formation of airborne polymers from photooxidation of aromatic precursors by reaction of carbonyls and their hydrates is reported by Kalberer et al. (2004). Sun et al. (2010) report dimer formation in aqueous-phase reactions of different phenols, including guaiacol. Physico-chemical properties of those aerosols according to optical properties and functional groups are hardly reported.

The state-of-the-art model of atmospheric HULIS, since 20 years in use, is based on selected macromolecular structures with an aromatic or olefinic core (Mukai and Ambe, 1986). The large aromatic content of HULIS may origin from oxidative and non-oxidative particle-phase reactions of different precursors including aromatics (Kroll and Seinfeld, 2008). Gelencsér et al. (2003) report formation of light-absorbing organic matter from aromatic hydroxy-acids with hydroxyl radicals and suggest those products as HULIS. Hoffer et al. (2004) characterized the Fenton-reaction products of 3,5-dihydroxybenzoic acid with OH radicals as synthetic HULIS. Humic substances, especially commercial humic and fulvic acids (e.g. Suwannee River fulvic acid (SRFA)) seem to differ significantly from atmospheric HULIS, as reported by a detailed and critical review about the humic-like character of atmospheric HULIS (Graber and Rudich, 2006). Further, their preparation as aerosols in an aerosol smog-chamber is rather difficult. Thus, precursors are needed as in-situ model substances to generate SOA with HULIS qualities (Cowen and Al-Abadleh, 2009).

An appropriate candidate for SOA with HULIS-properties is catechol, which is also reported as a strong emission from open biomass burning (Hays et al., 2005) and fireplace combustion (Fine et al., 2002) leading to so-called biomass-burning organic aerosols (BBOA). Catechol is also known as pyrocatechol, 1,2-dihydroxybenzene or benzene-1,2-diol. It is the ortho isomer of the three isomeric benzenediols (Fig. 1). Catechol is also used as a model compound for soils (Huber et al., 2010). Fahimi et al. (2003) used different derivatives of benzene, including catechol to study

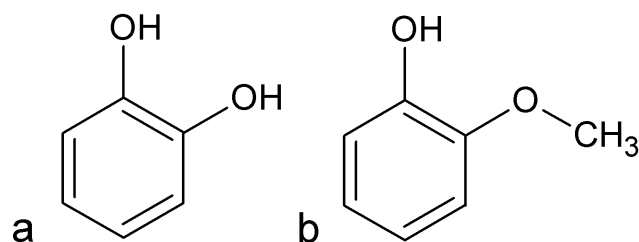


**Fig. 1.** The used SOA precursors: (a) catechol (Benzene-1,2-diol), (b) guaiacol (2-methoxyphenol)

the formation of chloroacetic acids. The transformation of catechol to humic polymers with the context of humus formation was studied by Ahn et al. (2006). Aerosol formation from catechol has been studied very recently (Coeur-Tourneur et al., 2009), obtaining large mass yields ranging from 17 to 86 wt.% in a smog-chamber in the presence of ozone with only minor influence of self-produced OH, which is known from scavenger experiments to enhance the consumption of catechol by 30% (Tomas et al., 2003). The rate constant for the reaction of catechol with  $\text{O}_3$  has been determined to be  $9.6 \times 10^{-18} \text{ cm}^3 \text{ s}^{-1}$  at 298 K, and the vicinal OH groups have been suggested as a potential cause of the high reactivity of catechol towards ozone (Tomas et al., 2003). The gas-phase reaction of dihydroxybenzenes with OH radicals has been studied in detail (Olariu et al., 2000). Furthermore, infrared spectroscopy of the oxidation of catechol has been performed in aqueous phase (Khovratovich et al., 1998). Aerosol flow reactor studies demonstrate ring-opening processes and formation of carboxylic acids located at aromatic or olefinic sites (Ofner et al., 2010). Nieto-Gligorovski et al. (2008, 2010) studied oxidation reactions of 4-carboxybenzophenone/catechol films using UV/VIS and FTIR spectroscopy. They report a photosensitized oxidation of the phenolic precursor by ozone in the presence of simulated sunlight to form products with properties similar to HULIS. Heterogeneous reactions of catechol aerosol with nitrogenous trace gases has been studied recently (Bröke et al., 2003). Also the methyl-ether modification of catechol, guaiacol, could be used to study aerosol formation. Guaiacol is also known as o-methoxyphenol, 2-methoxyphenol or methylcatechol (Fig. 1).

SOA from catechol and guaiacol has been chosen as a model system and has been analysed in time dependence under defined photochemical conditions in an aerosol smog-chamber. Different relative humidities have been simulated playing an important role in aerosol formation and/or processing (Vesna et al., 2009). A variety of methods is available to study atmospheric surfaces and their interaction with trace gases (Zellner et al., 2009). These methods show that surface functional groups play an important role for heterogeneous aerosol chemistry (Lary et al., 1999). For studying the formation and processing of those functional groups FTIR spectroscopy is most suitable (Najera et al., 2009).

Time resolved FTIR spectroscopy of the formation of organic aerosol particles was applied by Sax et al. (2005). Coury and Dillner (2008) used ATR-FTIR spectroscopy to quantify organic functional groups in ambient aerosols. Furthermore, light-absorption of organic materials plays an important role for the radiative forcing (Shapiro et al., 2009). To complete and confirm spectroscopic results ultrahigh resolution mass spectroscopy (ICR-FT/MS, Schmitt-Kopplin et al., 2010) and imaging by electron microscopy are used in the present study.

## 2 Methods

SOA, especially SOA with HULIS-properties, is a rather complex mixture of different organic macromolecules with various oxygenated functional groups. A single-molecule analysis has turned out to be rather useless. Therefore, in the focus of our analytic strategy are techniques which determine the functional groups, the O:C ratio, and the particle's morphology. Changes during the photo-oxidation shall be revealed and a well-characterized model substance will be defined.

### 2.1 Aerosol smog-chamber

All secondary organic aerosols were produced in a cylindrical 700 L aerosol smog-chamber made of Duran glass. Fluorinated ethylene propylene film (FEP) covers both ends of the cylinder and serves as window for a solar simulator, equipped with a medium-pressure metal vapour lamp (Osram HMI, 4000 W). A water cooled glass plate cuts off the UV-C range of the lamp spectrum. The one centimetre thick water film reduces the entry of infrared radiation from the HMI lamp into the smog-chamber. The principal setup of the aerosol smog-chamber has been described previously (Nolting et al., 1988). The current setup of the smog-chamber varies from the described one by increasing the volume by an additional 60-cm section to 700 L and thus changing the surface to volume ratio down to  $8.7 \text{ m}^{-1}$ . Further, the solar simulator is placed below the smog-chamber. Residence times of  $105 \pm 15$  min were measured for particles with diameters of  $50 \pm 5$  nm at simulated sunlight and 5–10 Pa overpressure.

The smog-chamber is flushed with particle-free air produced using a zero air generator (CMC ZA 50K). The ozone concentration at the beginning of the experiments was measured using a chemiluminescence ozone analyser (UPK 8002). The relative humidity was regulated at the beginning of the smog-chamber experiments by vaporizing a calculated amount of water. The Magnus equation (Sonntag, 1990) was used to calculate the saturated vapour pressure. The saturation gave access to the absolute amount of water, which was achieved based on a given relative humidity. The relative humidity was monitored using a Steinecker hydrometer (Type 49076D). The upper level of relative humidity available was

limited by the interference of water absorption in the long-path infrared absorption spectra.

The required amount of precursor was calculated with respect to the chamber volume, the pressure, and the temperature. Subsequently, the solid (catechol) or the liquid (guaiacol) precursor was filled into an impinger and then continuously vaporized and flushed into the chamber volume using the particle-free zero air. The chamber was permanently monitored using the CNC (described below in Sect. 2.2) to avoid particle formation during this filling procedure by supersaturation of the low-volatile precursors.

### 2.2 Aerosol size distribution

Aerosol particle concentrations were recorded using a CNC (TSI 3020). An electrostatic classifier (TSI 3071) with a neutralizer ( $^{85}\text{Kr}$ ), coupled to the CNC, was used to determine the aerosol size distribution.

### 2.3 Electron microscopy

Images of the formed aerosol particles were taken using a FEI Quanta 200 FEG-SEM. Particles were collected using Isopore<sup>TM</sup> membrane filters (Millipore) made of polycarbonate with a pore size of about 50 nm. The aerosol particles were protected against electric charging by sputtering 3–4 nm of Au/Pd onto their surface. The FEG-SEM was operating at  $6 \times 10^{-6}$  mbar using a cathode voltage of 5 kV to avoid high penetration depth and just image the surface.

### 2.4 Long-path FTIR spectroscopy

For long-path absorption, the chamber is equipped with a 40 m White-cell coupled to a FTIR spectrometer (Bruker IFS 113v). The instrument is evacuated down to 60 mbar to diminish disturbance of the spectra by atmospheric compounds. Long-path FTIR spectra were recorded at a spectral resolution of  $2 \text{ cm}^{-1}$  from 4000 to  $580 \text{ cm}^{-1}$  using a MCT detector and accumulating 256 single interferograms each. Post processing and atmospheric compensation of the infrared spectra was performed using the Bruker Opus software package (version 5.0).

### 2.5 Attenuated Total Reflectance (ATR) infrared spectroscopy

The aerosol particles were deposited onto the KRS-5 ATR crystal ( $52 \times 20 \times 2$  mm, trapezoidal) for ATR-FTIR spectroscopy between 4000 and  $400 \text{ cm}^{-1}$  using a self developed electrostatic precipitator (ESP). For sampling of aerosol particles onto a KRS-5 crystal, which was not possible with the former prototype described by Ofner et al. (2009), a two-stage precipitator was developed and is illustrated in Fig. 2. The precipitator is based on the concepts of Fierz et al. (2007) and Mainelis et al. (2002). This ESP has separate charging and deposition zones. The ESP is operated at high voltages

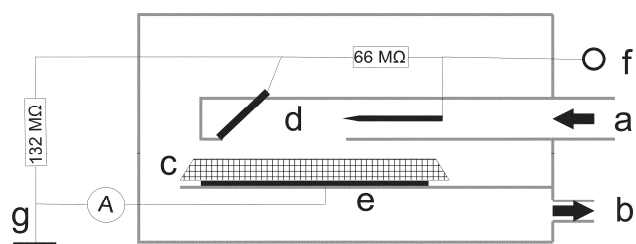


**Fig. 2.** Two-stage electrostatic precipitator for deposition of aerosol particles onto ATR crystals: (a) aerosol inlet; (b) vacuum pump (operated at a flow rate between  $0.3\text{--}3\text{ dm}^3\text{ min}^{-1}$ ); (c) ATR crystal; (d) charging and deposition zone; (e) copper electrode; (f) high voltage supply; (g) ground connection; A – electrometer for control of electric current flowing off the ATR crystal.

of about 10.5 kV. After entering the ESP the aerosol particles are charged by a corona effect and accelerated towards a bevelled deflector at 3.5 kV. The high voltage between the deflector and the ground plate of 7 kV turns the aerosol flight path towards the ATR crystal. Using an electrometer between the copper plate and the ground connection allows us to observe the electric current flowing off the ATR crystal (Fig. 2). For the ESP construction, the electric field between the needle, the deflector, and the ATR crystal was calculated using the software Student's QuickField 5.5 (Tera Analyses Ltd.).

The ATR spectra were recorded using a Bruker IFS 48 FTIR instrument with a Specac 25 reflection ATR optics. The spectral resolution of the infrared spectrometer was adjusted to  $4\text{ cm}^{-1}$ , and 512 interferograms with an optical range from 4000 to  $400\text{ cm}^{-1}$  were accumulated each for background and sample measurement. Post processing of the ATR spectra was performed by using the Bruker Opus software package.

## 2.6 UV/VIS spectroscopy

UV/VIS diffuse reflection spectra were recorded by a spectrophotometer (Uvikon XL, BIO-TEK Instruments) using an integrating Ulbricht sphere (Labsphere) between 200 and 800 nm at a speed of 200 nm per minute at a bandwidth of 4 nm. Aerosol samples were collected onto Whatman QMA quartz fibre filters. As reference material for the integrating sphere Labsphere Spectralon Diffuse Reflectance Standards were used (SRS-99-010). No significant absorption of UV/VIS radiation was observed comparing clean quartz fibre filters to the Labsphere standards.

## 2.7 TPP mass spectroscopy

This experiment has originally been developed at the Vienna University of Technology in order to analyse the oxidation processes of soot particles from diesel engines (Muckenhuber and Grothe, 2006; Ofner and Grothe, 2007). Soot is a multi-component system, which is extremely difficult to

analyse. Therefore, the focus has been set on the controlled fragmentation of the functional groups, which in fact are the key species when discussing reactivity. The same idea has been translated to the analyses of HULIS particles and their related oxidation processes. Aerosol particles were sampled onto quartz fibre filters mentioned above. In TPP-MS experiments the coated quartz fibre filters were placed in a quartz glass flask, which was evacuated down to  $10^{-5}$  bar. Then the sample was heated at high vacuum from room temperature up to  $900\text{ }^\circ\text{C}$  with a heating rate of  $10\text{ K min}^{-1}$ . Through a leak valve a small portion of the pyrolysis gases was induced into the UHV of the mass spectrometer (Balzers Prisma 200 QMS). Several mass fragments were recorded as a function of the pyrolysis temperature. To identify decomposing functional groups the mass signals of OH ( $m/z = 17$ ), CO ( $m/z = 28$ ) and  $\text{CO}_2$  ( $m/z = 44$ ) were exploited. Peaks were allocated to the decomposing functional groups (Muckenhuber and Grothe, 2006).

## 2.8 Ultrahigh resolution mass spectroscopy

Ultrahigh resolution mass spectroscopy was performed at the Helmholtz Centrum Munich, Germany with the Bruker 12 Tesla APEX Q Ion Cyclotron Resonance Fourier Transform Mass Spectrometer (Bremen, Germany). Electrospray injection was followed in negative mode with an APOLLO II electrospray source in flow injection at  $2\text{ }\mu\text{l/min}$  (Gaspar et al., 2009, and Schmitt-Kopplin et al., 2010). The molecular formulae were batch-calculated by a software tool, written in-house and achieving a maximum mass error of  $\leq 0.2$  ppm. The generated formulae were validated by setting sensible chemical constraints (N rule, O/C ratio  $\leq 1$ , H/C ratio  $\leq 2n + 2$ , element counts:  $\text{C} \leq 80$ , H unlimited,  $\text{O} \leq 60$ ) in conjunction with an automated theoretical isotope pattern comparison (Gaspar et al., 2009). Even enabling up to 3N and 3S resulted in mainly CHO types of elementary formulae (only few formulae corresponding to impurities were found as CHNO, CHOS and CHNOS, which are caused from the quartz filters.).

The filters were pushed by the cap into Eppendorf 2-ml vials, extracted directly with 1 ml of methanol and centrifuged in the same Eppendorf vials to be ready for injection.

## 3 Experimental

The precursors for the SOA were catechol (Riedel-de Haën, 32101, pro analysis grade,  $>99\%$  HPLC) and guaiacol (Sigma Aldrich, G5502, pro analysis grade,  $>99\%$  GC) (Fig. 1). Catechol has a molecular weight of  $110.11\text{ g mol}^{-1}$ , guaiacol of  $124.14\text{ g mol}^{-1}$ . Ozone was produced from pure oxygen (Riessner-Gase,  $>99,995\%$ ) using a silent discharge ozonizer (Sorbios, GSG 0012). For each precursor three experiments were carried out: (1) formation of SOA in the dark

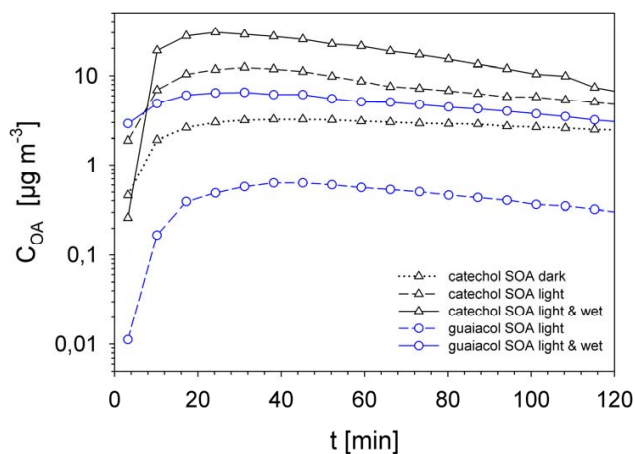


**Fig. 3.** Evolution of the particle mass concentration ( $C_{\text{OA}}$ ) over time: The catechol precursor causes higher aerosol mass yields than the guaiacol precursor. Particle formation is strongly influenced by environmental conditions like simulated sunlight and relative humidity.

with  $\text{O}_3$  only (0% relative humidity), (2) formation of SOA at simulated sunlight with  $\text{O}_3$  only (0% relative humidity) and (3) formation of SOA at simulated sunlight with  $\text{O}_3$  and 25% relative humidity. No particle formation could be observed from the reaction of guaiacol with  $\text{O}_3$  in the dark – hence no data is presented. For aerosol size distribution experiments, 100 ppb of the precursor and 500 ppb of ozone were used to study the formation of the SOA. FTIR experiments had to be performed at higher concentrations (5 ppm precursor substance and 20 ppm ozone) because of the detection limit of the long-path-FTIR spectrometer. ATR samples were collected onto the KRS-5 crystal two hours after SOA formation with duration of 30 min at an aerosol flow of  $6.5 \text{ cm}^3 \text{ s}^{-1}$ . About  $10^8$  aerosol particles were collected for each ATR measurements from medium particle concentrations of  $10^5 \text{ particles cm}^{-3}$  at a collection efficiency of about 90%. For UV/VIS spectroscopy, FEG-SEM imaging, TPP-MS, and ultrahigh resolution mass spectroscopy aerosol particles formed at higher precursor concentrations (5 ppm) were sampled onto the specified filter materials.

## 4 Results and discussion

### 4.1 Formation of SOA – aerosol size distribution and particle imaging

The mass concentrations and size distributions of the formed SOA strongly depend on the environmental conditions in the aerosol smog-chamber, as shown in Figs. 3 and 4. The aerosol mass distributions were derived from volume distributions with an assumed density of  $1.4 \text{ g cm}^{-3}$  (Coeur-Tourneur et al., 2009). Aerosol formation yields are influ-

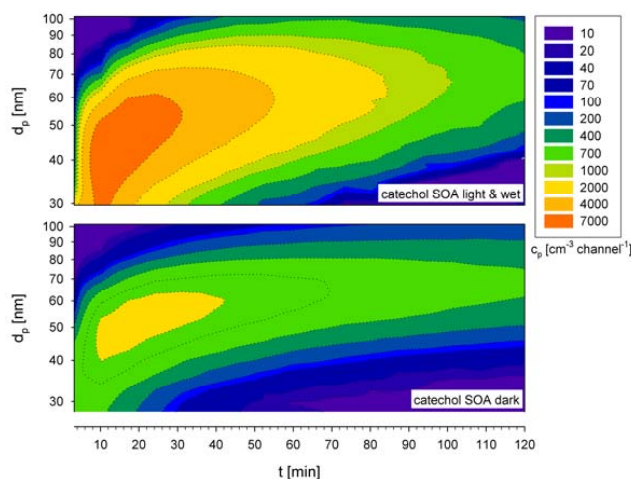


**Fig. 4.** Change of aerosol size distribution as a function of time: The formed particles reach final mean diameters of 65 nm (dark) and 70 nm (light and wet) after 2 h.

enced by the presence of simulated sunlight and relative humidity. The precursors play a decisive role in this formation process. The catechol precursor is found to generate one order of magnitude more aerosol mass than the guaiacol precursor at simulated sunlight conditions. At a relative humidity of 25% these yields are observed to increase significantly compared to the yields at dry conditions or without simulated sunlight. Particle size distributions show similar medium particle diameters for all experiments of  $50 \pm 5 \text{ nm}$ . The half-width of the particle size distribution from SOA produced in the dark ( $\sigma_g = 1.26$ ) is lower than that compared to the experiments of simulated sunlight ( $\sigma_g = 1.34$ ). The medium particle diameter of SOA formed from guaiacol at simulated sunlight and dry conditions is very low (32 nm).

Thus, UV/VIS radiation has an influence on particle formation, not only concerning the overall aerosol mass, but also concerning the particle size distribution as shown in Fig. 4. Particle formation seems to be fairly complete after about 30 min. Subsequently, only aggregation of small particles takes place, as demonstrated by the slow change of the aerosol diameters and the FEG-SEM image in Fig. 5.

For scanning electron microscopy (Fig. 5) higher precursor concentrations were selected to produce sufficient SOA particle density. Therefore, aerosol particles are slightly larger than the mean value observed in the aerosol size distributions (Figs. 3 and 4). The particles with diameters between 100 and 250 nm are of nearly perfect spherical morphology, indicating their airborne formation by gas-to-particle conversion (Pöschl et al., 2010). No structured surface texture is visible. Chain- and cluster-like aggregates of those particles have also been observed.

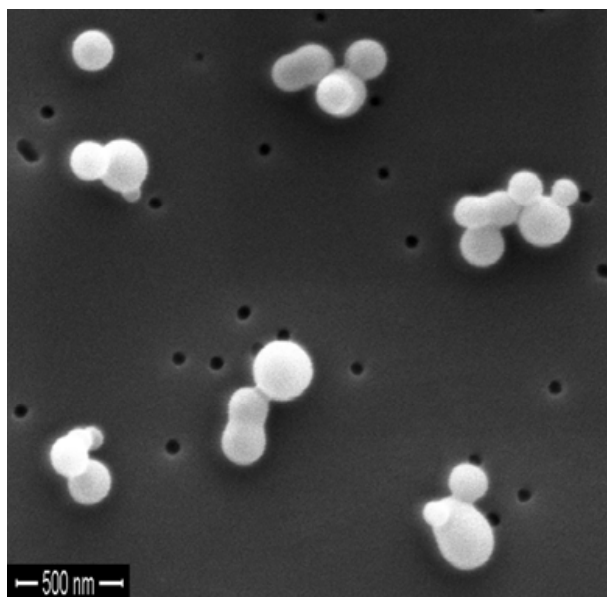


**Fig. 5.** FEG-SEM image of secondary organic aerosol particles on a polycarbonate filter: nearly perfect spherical particles with no visible surface texture form chain- and cluster-like aggregates. The spherical particles range in diameter from about 80 to 300 nm caused by an increased precursor concentration.

#### 4.2 Formation of SOA – long-path FTIR spectroscopy

During the aerosol formation process, the change of chemical bonds inside the aerosol particles has been studied by long-path FTIR spectroscopy using a 40 m White cell in the aerosol smog-chamber. Every 10 min 256 single scans were sampled. The medium residence time  $\tau$  of catechol in the smog-chamber was calculated to 10 min by observing the decrease of the aromatic stretch vibration at  $1510\text{ cm}^{-1}$ . Hence, during the first 10 min the precursor decays rapidly and products increase with approximately the same rate. After 30 min no further changes in the infrared spectrum are detectable. Thus, the SOA formation process of particles from catechol or guaiacol as precursors is completed after less than 30 min (Fig. 6). The chemical transformation of the precursor at the very beginning of the oxidation process (first 10 s) has been observed and discussed by Ofner et al. (2010). The formation of two main absorptions at  $1690$  and  $1755\text{ cm}^{-1}$  in the carbonyl stretching region is reported. Where the band at  $1690\text{ cm}^{-1}$  is occurring first and allocated to arylidic carbonyls and the band at  $1755\text{ cm}^{-1}$  is following, indicating ring-opened olefinic carbonyls. The long-path FTIR spectra from the aerosol smog-chamber indicate that the full-grown particles do not undergo any further oxidation. This can be well inspected by the carbonyl stretching vibration (see Fig. 6), which remains constant in shape and intensity. We conclude that the highly-polar, fully oxidized, gas-phase intermediates observed in the IR spectra are presumably the precursors of the SOA nucleation process.

According to the composition of the gas phase ( $\text{N}_2$ ,  $\text{O}_2$ ,  $\text{CO}_2$  and  $\text{O}_3$ ) and the chemical structure of the precursors, only vibrational modes containing carbon, oxygen, and hydrogen are expected. By the overlap of gaseous and solid products and gaseous educts, as well as other reactive or inert gas-phase species, a quantitative analysis of these data is hampered.

At the beginning of the SOA formation the spectra of the organic gas or particle phase can be assigned to the catechol molecule (Socrates, 1980). The aromatic ring exhibits typical aromatic  $\nu(\text{C}=\text{C})$  stretching vibrations at  $1620$ ,  $1510$  and  $1480\text{ cm}^{-1}$ . The sharp absorption at  $3063\text{ cm}^{-1}$  matches the  $\nu(\text{C}-\text{H})$  stretching vibration, the two absorptions at  $3671$  and  $3608$  are the respective  $\nu(\text{O}-\text{H})$ . Phenolic alcohols correspond to the vibrations at  $1364$  and  $1325\text{ cm}^{-1}$ , where the phenolic  $\nu(\text{C}-\text{O})$  stretching vibration can be found. The absorptions in the range  $1272$  to  $1155\text{ cm}^{-1}$  and the band at  $1090\text{ cm}^{-1}$  represent either the aromatic in-plane deformation  $\delta(\text{C}-\text{H})$  or the phenolic deformation mode  $\delta(\text{O}-\text{H})$ . The aromatic out-of-plane deformations are the absorptions between  $860$  and  $740\text{ cm}^{-1}$ . The ozone concentration is represented by the absorption at  $1043\text{ cm}^{-1}$ .

During the aerosol formation process most of those absorptions decrease and the formation of some new bands can be studied. The sharp maxima of the phenolic  $\nu(\text{O}-\text{H})$  vibration decrease, and new  $\nu(\text{O}-\text{H})$  vibrations are formed, indicated by the broad absorption at about  $3330\text{ cm}^{-1}$ . At the high-frequency shoulder of those bands the absorption at  $3450\text{ cm}^{-1}$  increases as well. This band might be assigned to the intra molecular bonded  $\nu(\text{OH})$  of  $-\text{O}\cdots\text{H}\cdots\text{O}=\text{}$ .

The aerosol particles are highly oxidized. This can be inspected by the strong carbonyl stretching vibration in the range  $1850$  to  $1680\text{ cm}^{-1}$ . Two main regions can be identified in this band, an absorption at  $1792\text{ cm}^{-1}$  indicating the  $\nu(\text{C}=\text{O})$  of esters, anhydrides and carboxylic acids and an absorption at  $1730\text{ cm}^{-1}$  indicating quinones, ketones and other aromatic and aliphatic  $\nu(\text{C}=\text{O})$  vibrations. More detailed characterization of the carbonyl stretching region was reported recently using an aerosol-flow-reactor coupled to an infrared transmission cell (Ofner et al., 2010).

The increasing vibration at  $1416\text{ cm}^{-1}$  is interpreted as the  $\delta(\text{O}-\text{H})$  deformation vibration in combination with the  $\nu(\text{C}-\text{O})$  stretching vibration of carboxylic acids or phenols. Strong hints at aliphatic or aromatic ether formation are given by the vibration at  $1118\text{ cm}^{-1}$ . This vibration might represent the aliphatic or aromatic  $\nu(\text{C}-\text{O})$  stretching vibration of ethers. The presence of carboxylic acids is underlined by the appearance of an absorption at  $955\text{ cm}^{-1}$  indicating the out-of-plane deformation mode  $\delta(\text{O}-\text{H})$ .

The decrease of the sharp maxima, which can be assigned to the aromatic ring vibrations, points at partial ring opening reactions. However, aromatic and unsaturated structures are still present in the resulting aerosol particles. Hence, the resulting organic molecules still contains higher oxidized benzene fragments.

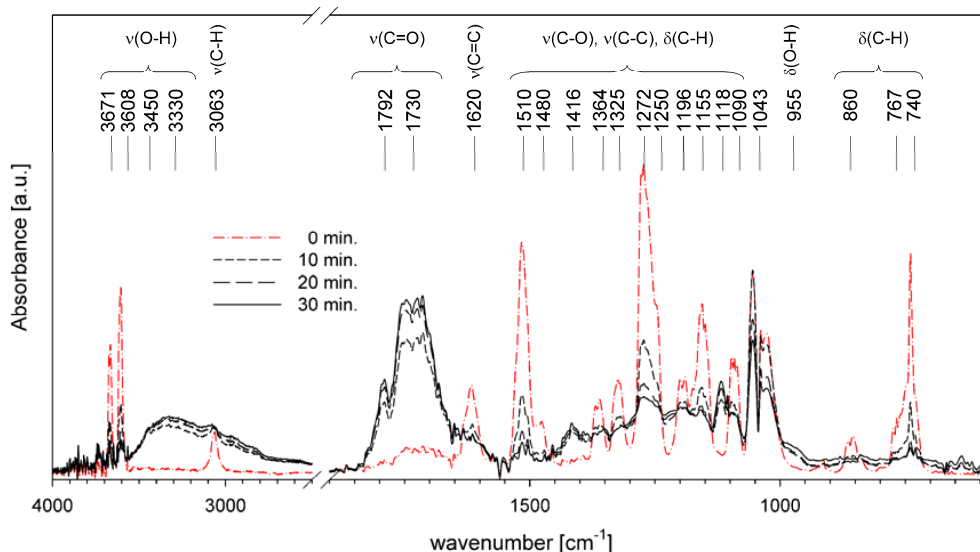


**Fig. 6.** Time resolved long path FTIR spectra of SOA formation from catechol with ozone in the dark: The well defined chemical structure of the precursor migrates to the broad rather undefined structure of macromolecular organic substances. Assignments of the observed bands are listed in Table 1.

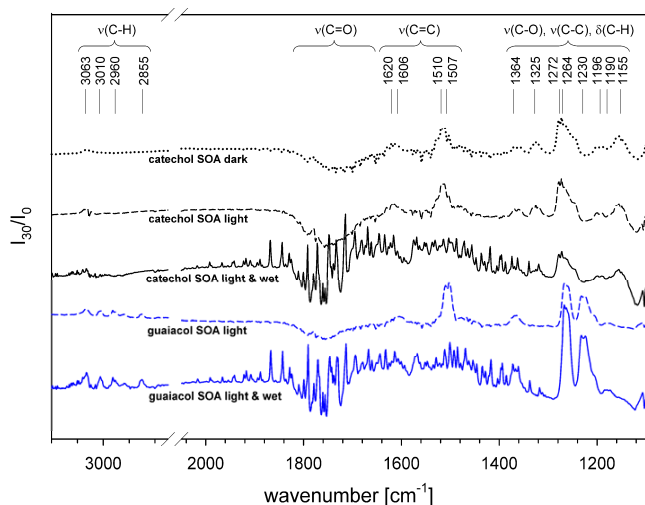


**Fig. 7.** Transmission difference spectra of the two aerosol precursors compared to the formed SOA at different ambient conditions after 30 min. The spectra are calculated by dividing the single spectra of the different aerosols after 30 min formation by the single spectra at the beginning of aerosol formation. Assignments of the observed bands are listed in Table 1.

Comparing the infrared transmission spectra of organic aerosols formed at different ambient conditions highlights functional differences not only because of the different precursors but also because of the varied experimental conditions (Fig. 7). The  $\nu(\text{C-H})$  stretching vibration of the aromatic hydrogens at  $3063\text{ cm}^{-1}$  are stronger degraded at wet conditions. This band appears to be the strongest with the

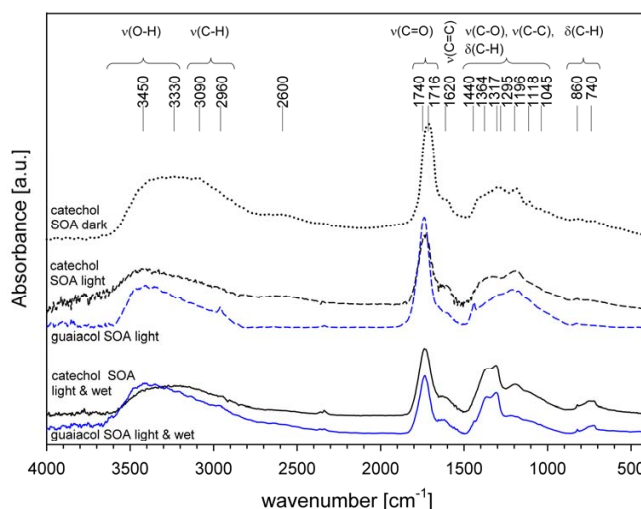


**Fig. 8.** ATR spectra of secondary organic aerosol particles from catechol and guaiacol sampled by electrostatic precipitation onto the KRS-5 crystal. Assignments of the observed bands are listed in Table 1.

“wet” guaiacol aerosol, because of the weak structure of the aromatic ring caused by the methyl ether group. The absorptions at  $3010$ ,  $2960$  and  $2855\text{ cm}^{-1}$ , which only appear in the guaiacol aerosol, are allocated to the methyl ether group. This group is lost during the aerosol formation process – strongest at wet conditions. Carbonyl containing functional groups implying  $\nu(\text{C=O})$  between  $1850$  and  $1690\text{ cm}^{-1}$  cannot be characterized in detail. The  $\nu(\text{C=C})$  stretching vibration of the aromatic ring at  $1620\text{ cm}^{-1}$  for the

catechol aerosol is red-shifted to  $1606\text{ cm}^{-1}$  for the guaiacol aerosol because of the enhanced total mass of the precursor molecule. The same shift appears for the aromatic stretching vibration at  $1510\text{ cm}^{-1}$  to  $1507\text{ cm}^{-1}$ .

The degradation of the phenolic group at  $1364$  and  $1325\text{ cm}^{-1}$  is visible for all five ambient conditions, although the band at  $1325\text{ cm}^{-1}$  is not visible in the spectra of guaiacol aerosol. The aromatic ring deformation modes at  $1272$  and  $1155\text{ cm}^{-1}$  also degrade during the conversion of the precursor. Differences within this frequency range agree with the lowered symmetry of guaiacol. Similar to the formation process of catechol and guaiacol aerosol are the degradation processes of main structural elements and entire functionalities. Main differences can be explained by the additional methyl-ether of guaiacol and therefore by the reduced symmetry and increased mass of the precursor.

### 4.3 ATR infrared spectroscopy of aerosol particles

Different formation pathways of SOA from catechol lead to different chemical properties of the formed aerosol (Fig. 8). According to the long-path FTIR spectra the major absorptions can be assigned the same way.

The aromatic structure of the SOA is indicated by the  $\text{C}=\text{C}$  – aromatic stretch at  $1620\text{ cm}^{-1}$ . Also a broad absorption in the range of the aromatic  $\text{C}-\text{H}$  stretch ( $3100\text{--}3000\text{ cm}^{-1}$ ) verifies this assumption. The aliphatic  $\text{C}-\text{H}$  stretch vibration is less pronounced at  $2960\text{ cm}^{-1}$  in the guaiacol aerosol. Also the absorptions at  $860$  and  $740\text{ cm}^{-1}$  of the  $=\text{C}-\text{H}$  out-of-plane deformations belong to the aromatic system of the organic aerosol.

SOA from catechol formed without solar simulation at 0% relative humidity exhibits  $\text{C}=\text{O}$  stretch vibration at  $1716\text{ cm}^{-1}$ . This band indicates aryl-aldehydes,  $\alpha,\beta$ -unsaturated carboxylic acids,  $\alpha,\beta$ -unsaturated aldehydes and  $\alpha,\beta$ -unsaturated esters. At simulated sunlight conditions this band shifts to  $1740\text{ cm}^{-1}$ , where the vibrations of saturated ketones, aldehydes, and esters are located. Aromatic or  $\alpha,\beta$ -unsaturated esters in the dark-formed SOA might be indicated by the bands at  $1716$ ,  $1295$ ,  $1196$  and  $1118\text{ cm}^{-1}$ . Carboxylic acids are represented by the  $\nu(\text{C}=\text{O})$  at  $1740\text{ cm}^{-1}$ , the  $\nu(\text{C}-\text{O})$  and  $\delta(\text{O}-\text{H})$  at  $1416$ ,  $1317$  and  $1295\text{ cm}^{-1}$  and the broad  $\nu(\text{O}-\text{H})$  from  $3100$  to  $2500\text{ cm}^{-1}$ . The  $\nu(\text{O}-\text{H})$  absorption below  $3000\text{ cm}^{-1}$  coupled to the carbonyl stretch at low wavenumbers observed for all samples gives also hints at carboxylic acid dimer formation (Excoffon and Marechal, 1972; Florio et al., 2003).

Absorptions in the range of  $3200\text{--}2500\text{ cm}^{-1}$  might belong to intramolecular-bonded ortho-phenols and the  $\text{O}-\text{H}$  stretch vibration of carboxylic acids. The broad structured absorption between  $1400$  and  $1000\text{ cm}^{-1}$  implies  $\text{O}-\text{H}$  deformation and  $\text{C}-\text{O}$  stretch vibration combinations of aliphatic and aromatic alcohols. The band at  $1196\text{ cm}^{-1}$  might – apart from structural features – also belong to the  $\text{C}-\text{O}$  stretch vibration in aromatic ethers or phenols, shown by all SOA sam-

ples. Hence, the absorption at  $1045\text{ cm}^{-1}$ , which is masked by ozone in the long-path absorption spectra, might belong to the  $\text{C}-\text{O}$  aliphatic stretch vibration of aliphatic-aromatic ethers. Same absorptions of carbonyls and aromatic rings were found for photodegraded tannic acid as a model for HULIS (Cowen and Al-Abadleh, 2009) or for SRFA (Hatch et al., 2009).

ATR-spectra of SOA from guaiacol imply the asymmetric stretch ( $2960\text{ cm}^{-1}$ ) and asymmetric deformation ( $1440\text{ cm}^{-1}$ ) of the  $-\text{CH}_3$  group. The intensity of those vibrations are reduced at wet conditions, because the  $-\text{CH}_3$  group is destroyed by the reaction with the  $\text{OH}$  radicals. The assignment of all other bands can be performed in the same way as for the catechol experiment. The combination of these two different FTIR methods allows us to allocate infrared group-frequencies to the functional groups and structural elements listed in Table 1.

ATR-FTIR spectra of SOA from catechol and guaiacol exhibit absorptions reported for natural HULIS and used proxies like SRFA. The carbonyl and aromatic stretching region between  $1600$  and  $1800\text{ cm}^{-1}$  are dominated by two bands at  $1620$  and  $1716$  or  $1740\text{ cm}^{-1}$ . Those absorptions are reported for SRFA and for natural HULIS (Salma et al., 2010). Especially the  $\nu(\text{C}=\text{O})$  at  $1716\text{ cm}^{-1}$  of SOA catechol formed in the dark was found in BBOA (Salma et al., 2010). Most important functional groups of SOA from catechol and guaiacol seem to be carboxylic acids, carboxylic anhydrides and lactones or esters, shown by ATR absorptions at  $1317$  and  $1295\text{ cm}^{-1}$  and TPP-MS. Those groups are reported for an ambient aerosol at a rural site with aromatic content of 17% (Coury and Dillner, 2009). Samburova et al. (2007) found high carboxylic and aryl fractions in HULIS samples. Aromatic acids with high-molecular weights were well correlated with HULIS by Stone et al. (2009). Carboxylic acids and their modifications are highly reported for natural HULIS, biomass burning aerosol and water-soluble organic carbon (WSOC) (Salma and Lang, 2008; Kundu et al., 2010; Limbeck and Puxbaum, 1999; Kumagai et al., 2010). While Sun et al. (2010) report dimer formation based on  $\text{C}-\text{O}$  or  $\text{C}-\text{C}$ , ATR-FTIR spectra from catechol and guaiacol give also hints on formation of carboxylic acid dimers. SOA was produced for FTIR and TPP-MS measurements at elevated concentrations, as described in the experimental section. This was not causing any identifiable discrepancies, when comparing with natural samples or other HULIS models.

In principle, all spectra of natural HULIS look rather similar, which is not surprising since these are mixtures of highly oxidized organic compounds. Small differences in band positions and relative intensities are related to the respective sampling site and the history of the aerosol. The main group frequencies of SOA ( $\nu(\text{O}-\text{H})$ ,  $\nu(\text{C}=\text{O})$ ,  $\nu(\text{C}=\text{C})_{\text{aromatic}}$ ,  $\nu(\text{C}-\text{O})$  of carboxylic acids and of ethers) from catechol and guaiacol are compared to natural HULIS extracts (Polidori et al., 2008; Duarte et al., 2005) and SRFA (Graber and Rudich, 2006), fulvic acids from soil (Stevenson and Goh, 1971)

**Table 1.** Main infrared group-frequencies [ $\text{cm}^{-1}$ ] assigned to functional groups\* and structural features observed in SOA from catechol and guaiacol at different ambient conditions by comparing aerosol-smog-chamber long-path FTIR spectra (LP) with ATR spectra (ATR). (w = weak, m = medium, s = strong)

Assignments	overall structure	catechol SOA			guaiacol SOA	
		dark	light	light and wet	light	light and wet
$\nu(\text{O-H})$ intramolec. and $-\text{COOH}$	3450	m	m	m	m	m
$\nu(\text{O-H})$	3330	m	m	m	m	m
$\nu(\text{C-H})$ aromatic	3063 <sub>LP</sub> 3090 <sub>ATR</sub>	m	w	m	w	w
$\nu(\text{C-H})$ of $-\text{CH}_x$	2960				m	w
R/Ar-COOH ··· HOOC-R/Ar	3000-2600 <sub>ATR</sub>	m	w	w	w	w
$\nu(\text{C=O})$ aryl and unsaturated	ATR	1716				
$\nu(\text{C=O})$ olefinic and saturated	ATR		1740	1740	1740	1740
$\nu(\text{C=C})$ aromatic, olefinic	LP	1620	1620	1620	1606	1606
$\nu(\text{C=C})$ aromatic ring vibr.	LP	1510	1510	1510	1507	1507
$\delta(\text{C-H})$ of $-\text{CH}_x$	1440 <sub>ATR</sub>				m	w
$\nu(\text{C-O})$ and $\delta(\text{O-H})$ of $-\text{COOH}$	1416 <sub>LP</sub>	s	s	m	m	m
$\nu(\text{C-O})$ of $-\text{OH}$	1364	m	m	m	s	s
$\nu(\text{C-O})$ of $-\text{COOH}$ , R-COO-R	1317 <sub>ATR</sub> 1295 <sub>ATR</sub>	s	m	m	s	s
$\nu(\text{C-O})$ of Ar-O-Ar, Ar-OH or R-COO-R	1196	s	s	m	s	m
$\nu(\text{C-O})$ of R-O-Ar	1118	m	w	w	w	w
$\nu(\text{C-O})$ of R-O-Ar or R-O-R	1045	m	m	m	m	m
$\delta(\text{O-H})$ carboxylic acids	955 <sub>LP</sub>	m	w	w	w	w
$\delta(\text{C-H})$ out-of-plane	860, 740	m	w	w	s	s

\* Ar – representing conjugated or aromatic structural elements.  
R – representing aliphatic or substituted olefinic structural elements.

**Table 2.** Comparison of the band positions [ $\text{cm}^{-1}$ ] and strengths (w = weak, m = medium, s = strong) of the present ATR-FTIR spectra of SOA from catechol and guaiacol with IR spectra of natural humic and fulvic acids and HULIS and other HULIS models.

Material Assignments	Natural humic and fulvic acids <sup>(1)</sup>	Natural humic and fulvic acids <sup>(2)</sup>	Extracts from rural aerosol <sup>(3)</sup>	Extracts from urban aerosol <sup>(4)</sup>	Tannic acid as model for HULIS <sup>(5)</sup>	SOA from catechol and guaiacol (this work)
$\nu(\text{O-H})$ aromatic	3400	3300–3400	3400 m	3360–3444 m	3392–3400 m	3330–3450 m
$\nu(\text{C=O})$	1720 m	1720	1720 s	1710–1742 s	1713 m	1716–1740 s
$\nu(\text{C=C})$	1600–1660	1620	1600–1660 m	1613–1638 m <sup>(a)</sup>	1616 m	1620 m
$\nu(\text{C-O})$ of $-\text{COOH}$	~ 1200	1225, 1350	1220	1439, 1375 <sup>(c)</sup>	1209, 1298, 1250–1310	1295, 1317, 1416
$\nu(\text{C-O})$ of ethers	1050 <sup>(a)</sup>	–	1061 <sup>(b)</sup>	1045, 1090, 1177, 1217 w	1036, 1045 and 1080 w	1045 and 1118 w

<sup>(a)</sup> interpreted as  $\nu(\text{C=O})$  alone; <sup>(b)</sup> assigned to polysaccharides; <sup>(c)</sup> allocated to  $\text{COO}^-$  <sup>(1)</sup> Stevenson and Goh (1971); IR spectra from KBr pellets containing aqueous extracts of humic and fulvic acids from various soils, mud and peat. <sup>(2)</sup> Baes and Bloom (1989); DRIFT spectra of powders, material was extracted from peat. <sup>(3)</sup> Graber and Rudich (2006); comparing the FTIR spectrum Suwannee River fulvic acid standard reference material ([www.ihss.gatech.edu](http://www.ihss.gatech.edu)) with HULIS: aqueous extracts from aerosol at a rural area in Portugal (summer and autumn) presented by Duarte et al. (2005). <sup>(4)</sup> Polidori et al. (2008); ATR-FTIR spectra of various extracts (hexane, dichloromethane, ethyl acetate, acetone and methanol) from aerosol collected at Pittsburgh in spring/summer and fall/winter. <sup>(5)</sup> Cowen and Al-Abadleh (2009); DRIFTS spectra of tannic acid (as a model for HULIS) and its photodegradation products.

and peat humic and fulvic acids (Baes and Bloom, 1989) as well as to tannic acid, which is a previously reported model compound (Cowen and Al-Abadleh, 2009) (see Table 2). The main characteristic frequencies are assigned in the same way as in the literature. However, in two studies (Polidori et al., 2008; Stevenson and Goh, 1971) the absorption at about  $1620 \text{ cm}^{-1}$ , which is present also in all our spectra, has been interpreted as an additional  $\nu(\text{C=O})$  band. Based on our long-path spectra and according to Graber and Rudich (2006) and Cowen and Al-Abadleh (2009) an assignment to  $\nu(\text{C=C})$ , maybe in resonance with  $\nu(\text{C=O})$ , seems to

be the more comprehensible interpretation – an amide band, as found in some field samples, cannot be present in our lab studies where nitrogen-containing compounds are absent. While the main absorptions are in excellent agreement, differences occur only for the assignment of  $\nu(\text{C-O})$  of the carboxylic acids between all five studies. The different positions are compared in Table 2. The reason for that might be the different degree of dissociation of the carboxylic acids or a possible hydrogen bonding depending on the environmental conditions and ester- carboxylic-acid-dimer-like molecular structures.

**Table 3.** Maxima of observed decomposition temperatures [ $^{\circ}\text{C}$ ] of functional groups in a sample of catechol SOA dark (bold face, s = strong, w = weak) and comparison with the other conditions (light, light and wet) and precursor\*, leading to the categories increased ( $\uparrow$ ), equal ( $=$ ), decreased ( $\downarrow$ ) and not observed ( $-$ ) for the functional groups.

Functional groups	carboxylic acids	carboxylic anhydride	lactones and esters	phenols	ethers	carbonyls and quinones
Decomposition temperatures	270 / 320	460	620	680	680	860
<b>catechol dark</b>	<b>s / w</b>	<b>w</b>	<b>s</b>	<b>w</b>	<b>w</b>	<b>s</b>
catechol light	$\downarrow$ / $=$	$\uparrow$	$=$	$=$	$=$	$\downarrow$
catechol light and wet	$\downarrow$ / $\uparrow$	$=$	$=$	$\uparrow$	$=$	$\downarrow$
guaiacol light	$=$ / $\uparrow$	$\uparrow$	$=$	$=$	$=$	$-$
guaiacol light & wet	$\downarrow$ / $\uparrow$	$=$	$\downarrow$	$=$	$=$	$\downarrow$

\* Data concerning guaiacol SOA in dark do not exist because of a lack of reactivity against ozone.

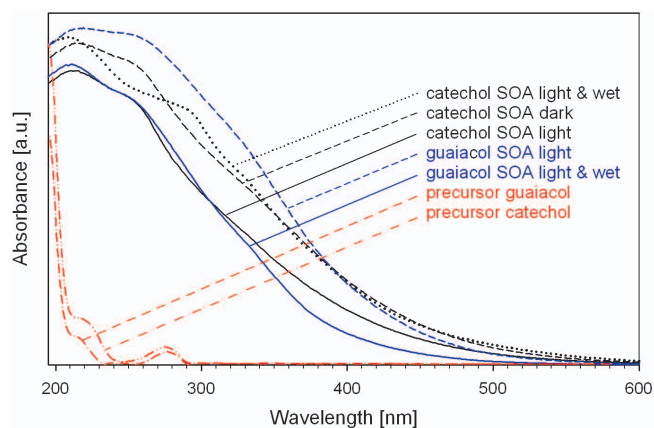


**Fig. 9.** Diffuse reflectance UV/VIS spectra of SOA from catechol and guaiacol and absorption spectra of the pure compounds.

#### 4.4 Diffuse reflectance UV/VIS spectroscopy of aerosol particles

The diffuse reflectance UV/VIS spectra of the different aerosol particles from catechol and guaiacol are dominated by a broad, typical Ångström absorption coefficient behaviour (Moosmüller et al., 2010) detectable up to 600 nm, which is in good agreement with the brown colour of these samples (Fig. 9). The broadness is such that individual electronic transitions can hardly be distinguished, underlining the fact that numerous types of conjugated  $\pi$  bonds exist in the SOA. The main absorptions of the two precursors catechol and guaiacol in the UV/VIS range are at about 220 and 275 nm, related to the  $\pi \rightarrow \pi^*$  transition of the aromatic system and the  $n \rightarrow \pi^*$  transition of the lone pairs of the hydroxyl substituent. Within the broad absorption of the organic aerosol particles there occur three main absorptions at 212, 254 and 333 nm, which are represented in all different types of organic aerosol from catechol and guaiacol. One additional absorption at 292 nm is only represented in the catechol dark SOA. This transition seems to be destroyed by UV/VIS radiation.

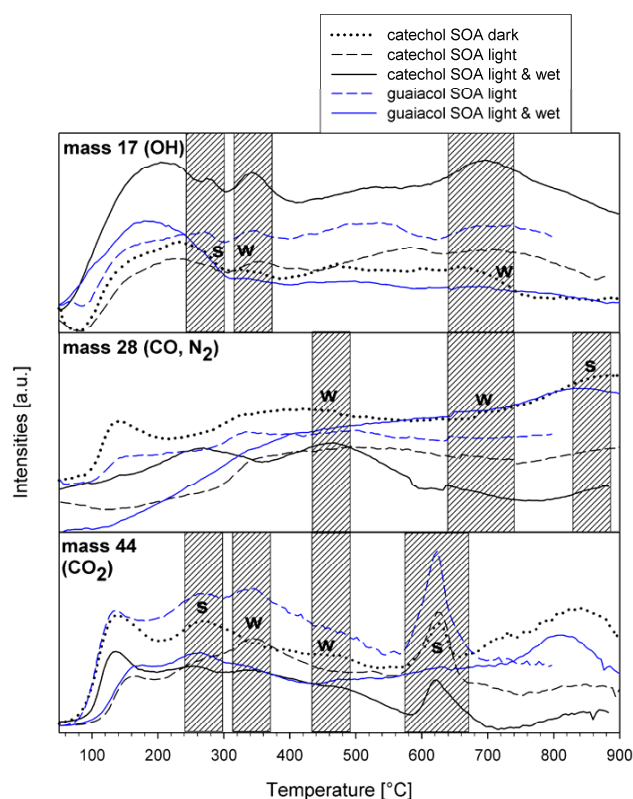


**Fig. 10.** TPP signals of the three important masses 17 (OH), 28 (CO or  $\text{N}_2$ ) and 44 ( $\text{CO}_2$ ) observed as a function of temperature for the five different SOA particles. The hatched temperature ranges mark observed decomposition of the following functional groups in soot: carboxylic acid (270 and 320), carboxylic acid anhydride (460), lactone and ester (620), phenol (680,  $m/z = 17$ ), ether (680;  $m/z = 28$ ), and carbonyl and quinone (860). The strengths of these features are indicated as s (strong) and w (weak) for catechol SOA dark, and are compared with each other SOA in Table 3.

The UV/VIS spectra are in well agreement with other aromatic precursor oxidation studies (Gelencsér et al., 2003; Hoffer et al., 2004). Especially the  $\pi \rightarrow \pi^*$  electron transition at about 260 nm is similar to natural HULIS samples (Baduel et al., 2009).

#### 4.5 TPP-MS of solid aerosol phase

The background corrected TPP mass spectra of the five aerosol types are well structured for the masses 17 (OH), 28 (CO) and 44 (CO<sub>2</sub>) (Fig. 10). Peaks below 150 °C are not interpreted because of outgassing of physically adsorbed molecules like H<sub>2</sub>O, N<sub>2</sub>, CO and CO<sub>2</sub> which might pollute the signals of pyrolysing functional groups. Based on the thermal stability of oxygen containing functional groups and their fragments (Muckenhuber and Grothe, 2006) peak maxima and relative peak intensities have been assigned to the different aerosol types (Table 3).

Two thermal instabilities of carboxylic acids occur at 270 and 340 °C. There are small differences in the relative intensities of those two acids. The *m/z* 44 signal assigned to lactones or esters is very intense for all aerosol particles except guaiacol SOA light and wet. Further carboxylic anhydrides, phenols and carbonyls and quinones are represented in the TPP mass spectra. Ethers might decompose at 680 °C, but the resulting *m/z* 28 signal is rather small.

The thermal analysis of functional groups is in good agreement with the vibrational spectra, confirming that highly oxidized functional groups play a major role but demonstrating that also lower oxidized groups are present in the aerosol particles. While enhancing the oxidation ability by changing the environmental conditions, carboxylic acids which are stable at higher temperatures (320 °C) increase. However, carboxylic acids at lower temperatures (270 °C), carbonyls and quinones decrease. Minor increases could be observed at carboxylic anhydrides and phenols. The amount of lactones or esters seems to be stable at different simulated environmental situations.

#### 4.6 Ultrahigh resolved mass spectra of aerosol composition

The methanol extracts from the filter samples exhibit a Gaussian signal distribution between 150 and 900 *m/z* (Fig. 11a) in negative mode electrospray ICR-FT/MS. The main region is between 200 and 450 *m/z*. The polymers showed thousands of signals that are calculated into individual CHO elementary compositions. In the presence of light, the chemical diversity of the samples significantly increased for both catechol- and guaiacol-based mixtures; water however did not have the same impact. The main *m/z* ratio of organic molecules in the particles of 200–450 is closer to natural HULIS samples than SRFA (Graber and Rudich, 2006) and is comparable to other SOA samples from photooxidation (Kalberer et al., 2004; Schmitt-Kopplin et al., 2010).

The distribution of the *m/z* signal in ICR-FT/MS is very similar between the catechol- and guaiacol-aerosol extracts. A detailed description on the elementary composition level shows signals that are typical of the catechol or guaiacol origin.

Hundreds of calculated elementary compositions were transformed into atomic H/C and O/C ratios for a representation on Van Krevelen Diagrams (Hertkorn et al., 2007; Hertkorn et al., 2008). Based on only one molecular precursor the resulting aerosols cover a major part of the possible CHO compositional space. Previous ICR-FT/MS analysis on organic aerosols obtained from chamber experiments based on  $\alpha$ -pinene ozonolysis enabled the differentiation of various monomers to oligomers (Reinhard et al., 2007); in this case however the mixtures are characteristic with continuous H/C values restricted between 0.5 and 1.5 and O/C values ranging from 0.3 up to 1 with gradual changes in peak intensity with increasing oxygen content. This behaviour is particular to the catalyzed oxidative polymerisation of these phenols to polyphenols as described in the early days of soil humic substance chemistry (Stevenson, 1994). Organic aerosol from catechol and guaiacol is typically characterized by high oxygen to carbon ratios (Fig. 11b), indicating the presence of highly-oxidized benzenes or conjugated olefins. Catechol-based mixtures also significantly differ from guaiacol (Fig. 11b) with signals of increased intensity having lower oxygen content and higher aromaticity. The O/C ratio between 0.3 and 1 is in good agreement with the reported O/C ratios for LV-OOA (low-volatile oxidized organic aerosol) and SV-OOA (semi-volatile OOA) (Jimenez et al., 2009). Further, the medium value of 0.6–0.7 fits the described oxidation state of atmospheric HULIS very well, although the measured H/C ratio of about 1 is lower than the reported 1.6–1.7 (Graber and Rudich, 2006). The H/C ratio is in good agreement with the widely used proxy SFRA (Dinar et al., 2006).

Based on the chemical structure of the precursors, hydrogen to carbon ratios above 1 and high oxygen contents can only be explained by condensations and the addition of hydroxyl groups to the unsaturated carbon structure, which is confirmed by the broad  $\nu(\text{O-H})$  absorption in the FTIR spectra.

## 5 Conclusions

SOA from catechol and guaiacol typically exhibits small particles with diameters between 40 and 90 nm, built up by a very fast formation process. Environmental conditions like solar radiation or relative humidity influence not only physical properties like aerosol size distributions or formation yields but also chemical properties like the total amount of oxidized sites and amount and types of functional groups.

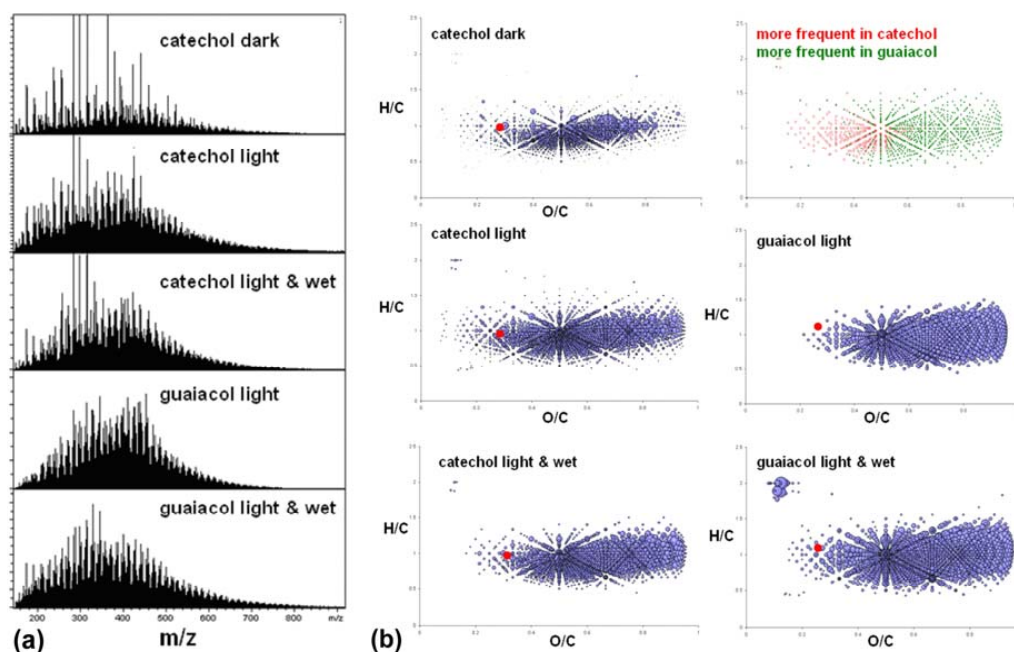


**Fig. 11.** ICR-FT/MS spectra in the  $m/z$  range 150 to 900 (a) and Van Krevelen diagrams (b) showing the distribution of the H/C and O/C ratios of the ICR-FT/MS data in the CHO compositional space as a function of precursor, light and wet.

The difference between the H/C values is explained by the absence of aliphatic side chains in the SOA from catechol and guaiacol. Hence, SOA from those precursors represents the aromatic and olefinic oxidized core structure of atmospheric HULIS very well. Only saturated aliphatic parts of atmospheric HULIS are not represented.

Light absorption of those organic particles ranges from less than 200 nm up to 600 nm into the visible region and declines very smoothly. Thus, derived SOA samples are light brown coloured. This optical feature indicates absorption processes according to aromatic or olefinic structures with a large variety of chemically bonded oxygen.

The chemical transformation from the gaseous precursor to the final aerosol particle is distinguished by the formation of different functional groups and disappearance of well defined structural elements of the entire benzene ring. The aromatic or olefinic structural element, an important attribute for atmospheric HULIS, still persists in the aerosol particle.

The variation of simulated sunlight or relative humidity results in various degrading structural elements like aromatic  $\nu(\text{C}=\text{C})$  and  $\nu(\text{C}-\text{H})$  stretch vibrations and pronounced oxygen containing functional groups, shifting  $\nu(\text{C}=\text{O})$  vibrations.

SOA from catechol and guaiacol provides several features according to natural and synthetic HULIS and commercial proxies as discussed above. Especially the high molecular weight caused by the aromatic system and the polycarboxylic acidic functionality matches those properties. Also the main reported group frequencies are well comparable to humic acids, natural HULIS and other model HULIS.

Due to the easy preparation, our model is applicable for lab-scale measurements of organic aerosol processing in an aerosol smog-chambers or aerosol flow reactors. Commercial HULIS proxies like SRFA would need special and complex preparation techniques like ultra-sonic nebulising or atomizing of solutions. While the use of one precursor allocation with comparable properties and even permits formation under very different simulated environmental situations easy aerosol preparations. SOA could perform like SV- and LV-OOA using aerosol-smog-chamber experiments close to natural conditions. Different stable aged modifications of SOA from catechol and guaiacol could be obtained. Synthetic SOA from catechol and guaiacol produced in aerosol smog-chamber experiments fulfil the physical chemical characteristics of HULIS better than SRFA due to their analytical properties and can be used as atmospheric model substances for HULIS in laboratory experiments to study heterogeneous reactions with aromatic or olefinic cores.

*Acknowledgements.* This work was supported by the Deutsche Forschungsgemeinschaft within the HALOPROC project and by the European Union within the EUROCHAMP project.

Edited by: V. F. McNeill

## References

- Ahn, M.-Y., Martínez, C. E., Archibald, D. D., Zimmermann, A. R., Bollag, J.-M., and Dec, J.: Transformation of catechol in the presence of a laccase and birnessite, *Soil Bio. Biochem.*, **38**, 1015–1020, 2006.
- Andreae, M. O. and Crutzen, P. J.: Atmospheric aerosols: biogeochemical sources and role in atmospheric chemistry, *Science*, **276**, 1052–1058, 1997.
- Andreae, M. O.: A new look at aging aerosols, *Science*, **326**, 1493–1494, 2009.
- Baduel, C., Voisin, D., and Jaffrezo, J. L.: Comparison of analytical methods for Humic Like Substances (HULIS) measurements in atmospheric particles, *Atmos. Chem. Phys.*, **9**, 5949–5962, doi:10.5194/acp-9-5949-2009, 2009.
- Baes, A. U. and Bloom, P. R.: Diffuse reflectance and transmission Fourier transform infrared (DRIFT) spectroscopy of humic and fulvic acids, *Soil Sci. Soc. Am. J.*, **53**, 695–700, 1989.
- Bröske, R., Kleffmann, J., and Wiesen, P.: Heterogeneous conversion of NO<sub>2</sub> on secondary organic aerosol surfaces: A possible source of nitrous acid (HONO) in the atmosphere?, *Atmos. Chem. Phys.*, **3**, 469–474, doi:10.5194/acp-3-469-2003, 2003.
- Coeur-Tourneur, C., Tomas, A., Guilloteau, A., Henry, F., Ledoux, F., Visez, N., Riffault, V., Wenger, J. C., and Bedjanian, Y.: Aerosol formation yields from the reaction of catechol with ozone, *Atmos. Environ.*, **43**, 2360–2365, 2009.
- Coury, C. and Dillner, A. M.: A method to quantify organic functional groups and inorganic compounds in ambient aerosols using attenuated total reflectance FTIR spectroscopy and multivariate chemometric techniques, *Atmos. Environ.*, **42**, 5923–5932, 2008.
- Coury, C. and Dillner, A. M.: ATR-FTIR characterization of organic functional groups and inorganic ions in ambient aerosols at a rural site, *Atmos. Environ.*, **43**, 940–948, 2009.
- Cowen, S. and Al-Abadleh, H. A.: DRIFTS studies on the photodegradation of tannic acid as a model for HULIS in atmospheric aerosols, *Phys. Chem. Chem. Phys.*, **11**, 7838–7847, 2009.
- Dinar, E., Taraniuk, I., Graber, E. R., Katsman, S., Moise, T., Anttila, T., Mentel, T. F., and Rudich, Y.: Cloud Condensation Nuclei properties of model and atmospheric HULIS, *Atmos. Chem. Phys.*, **6**, 2465–2482, doi:10.5194/acp-6-2465-2006, 2006.
- Duarte, R., Pio, C. A., and Duarte, A. C.: Spectroscopic study of the water-soluble organic matter isolated from atmospheric aerosols collected under different atmospheric conditions, *Analyt. Chim. Acta*, **530**, 7–14, 2005.
- Excoffon, P. and Marechal, Y.: Infrared spectra of H-bonded systems: saturated carboxylic acid dimers, *Spectrochim. Acta*, **28A**, 269–283, 1972.
- Fahimi, I. J., Keppler, F., and Schöler, H. F.: Formation of chloroacetic acids from soil, humic acid and phenolic moieties, *Chemosphere*, **52**, 513–520, 2003.
- Fierz, M., Kaegi, R., and Burtscher, H.: Theoretical and experimental evaluation of a portable electrostatic TEM sampler, *Aerosol Sci. Technol.*, **41**, 520–528, 2007.
- Fine, P. M., Cass, G. R., and Simoneit, B. R. T.: Chemical characterization of fine particle emissions from the fireplace combustion of woods grown in the southern United States, *Environ. Sci. Technol.*, **36**, 1442–1451, 2002.
- Fisseha, R., Dommen, J., Sax, M., Paulsen, D., Kalberer, M., Maurer, R., Höfler, F., Weingartner, E., and Baltensberger, U.: Identification of organic acids in secondary organic aerosol and the corresponding gas phase from chamber experiments, *Anal. Chem.*, **76**, 6535–6540, 2004.
- Florio, G. M., Zwier, T. S., Myshakin, E. M., Jordan, K. D., and Sibert III, E. L.: Theoretical modelling of the OH stretch infrared spectrum of carboxylic acid dimers based on first-principles anharmonic couplings, *J. Chem. Phys.*, **118**, 1735–1746, 2003.
- Forster, P., Ramaswamy, V., Artaxo, P., Berntsen, T., Betts, R., Fahey, D. W., Haywood, J., Lean, J., Lowe, D. C., Myhre, G., Nanga, J., Prinn, R., Raga, G., Schulz M., and Van Dorland, R.: Changes in atmospheric constituents and in radiative forcing, in: *Climate Change 2007: The physical science basis. Contribution of working group I to the fourth assessment report of the intergovernmental panel on climate change*. edited by: Solomon, S., Qin, D., Manning, M., Chen, Z., Marquis, M., Averyt, K. B., Tignor, M., and Miller, H. L., Cambridge University Press, Cambridge, United Kingdom and New York, 2007.
- Forstner, H. J. L., Flagan, R. C., and Seinfeld, J. H.: Secondary organic aerosol from the photooxidation of aromatic hydrocarbons: Molecular composition, *Environ. Sci. Technol.*, **31**, 1345–1358, 1997.
- Gaspar, A., Kunenkov, E., Lock, R., Desor, M., Perminova, I., and Schmitt-Kopplin, Ph.: Combined utilization of ion mobility- and ultra high resolution-MS to identify multiply charged constituents in natural organic matter, *Rapid Com. Mass Spec.*, **23**, 683–688, 2009.
- Gelencsér, A., Hoffer, A., Kiss, G., Tombácz, E., Kurdi, R., and Bencze, L.: In-situ formation of light-absorbing organic matter in cloud water, *J. Atmos. Chem.*, **45**, 25–33, 2003.
- Graber, E. R. and Rudich, Y.: Atmospheric HULIS: How humic-like are they? A comprehensive and critical review, *Atmos. Chem. Phys.*, **6**, 729–753, doi:10.5194/acp-6-729-2006, 2006.
- Hallquist, M., Wenger, J. C., Baltensperger, U., Rudich, Y., Simpson, D., Claeys, M., Dommen, J., Donahue, N. M., George, C., Goldstein, A. H., Hamilton, J. F., Herrmann, H., Hoffmann, T., Iinuma, Y., Jang, M., Jenkin, M. E., Jimenez, J. L., Kiendler-Scharr, A., Maenhaut, W., McFiggans, G., Mentel, Th. F., Monod, A., Prvt, A. S. H., Seinfeld, J. H., Surratt, J. D., Szmigielski, R., and Wildt, J.: The formation, properties and impact of secondary organic aerosol: current and emerging issues, *Atmos. Chem. Phys.*, **9**, 5155–5236, doi:10.5194/acp-9-5155-2009, 2009.
- Hatch, C. D., Gierlus, K. M., Zahardis, J., Schuttlefield, J., and Grassian, V. H.: Water uptake of humic and fulvic acid: measurements and modelling using single parameter Köhler theory, *Environ. Chem.*, **6**, 380–388, 2009.
- Hays, M. D., Fine, P. M., Geron, C. D., Kleeman, M. J., and Gullett, B. K.: Open burning of agricultural biomass: Physical and chemical properties of particle-phase emissions, *Atmos. Environ.*, **39**, 6747–6764, 2005.
- Hertkorn N., Meringer, M., Gugisch, R., Ruecker, C., Frommberger, M., Perdue, E. M., Witt, M., and Schmitt-Kopplin, Ph.: High-precision frequency measurements: indispensable tools at the core of molecular-level analysis of complex systems, *Anal. Bioanal. Chem.*, **389**, 1311–1327, 2007.
- Hertkorn, N., Frommberger, M., Schmitt-Kopplin, Ph., Witt, M., Koch, B., and Perdue, E. M.: Natural organic matter and the

- event horizon of mass spectrometry, *Anal. Chem.*, 80, 8908–8919, 2008.
- Hoffer, A., Kiss, G., Blazsó, M. and Gelencsér, A.: Chemical characterization of humic-like substances (HULIS) formed from a lignin-type precursor in model cloud water, *Geophys. Res. Lett.*, 31, L06115/1–L06115/4, doi:10.1029/2003GL018962, 2004.
- Huber, S. G., Wunderlich, S., Schöler, H. F., and Williams, J.: Natural abiotic formation of furans in soil, *Environ. Sci. Technol.*, 44, 5799–5804, 2010.
- Iinuma, Y., Boge, O., Gnauk, T., and Herrmann, H.: Aerosol-chamber study of the  $\alpha$ -pinene/O<sub>3</sub> reaction: influence of particle acidity on aerosol yields and products, *Atmos. Environ.*, 38, 761–773, 2004.
- Jang, M., and Kamens, R. M.: Characterization of secondary aerosol from the photooxidation of toluene in the presence of NO<sub>x</sub> and 1-Propene, *Environ. Sci. Technol.*, 35, 3626–3639, 2001.
- Jimenez, J. L., Canagaratna, M. R., Donahue, N. M., Prevot, A. S. H., Zhang, Q., Kroll, J. H., DeCarlo, P. F., Allan, J. D., Coe, H., Ng, N. L., Aiken, A. C., Docherty, K. S., Ulbrich, I. M., Grieshop, A. P., Robinson, A. L., Duplissy, J., Smith, J. D., Wilson, K. R., Lanz, V. A., Hueglin, C., Sun, Y. L., Tian, J., Laaksonen, A., Raatikainen, T., Rautiainen, J., Vaattovaara, P., Ehn, M., Kulmala, M., Tomlinson, J. M., Collins, D. R., Cubison, M. J., Dunlea, J., Huffman, J. A., Onasch, T. B., Alfarra, M. R., Williams, P. I., Bower, K., Kondo, Y., Schneider, J., Drewnick, F., Borrmann, S., Weimer, S., Demerjian, K., Salcedo, D., Cottrell, L., Griffin, R., Takami, A., Miyoshi, T., Hatakeyama, S., Shimono, A., Sun, J. Y., Zhang, Y. M., Dzepina, K., Kimmel, J. R., Sueper, D., Jayne, J. T., Herndon, S. C., Trimborn, A. M., Williams, L. R., Wood, E. C., Middlebrook, A. M., Kolb, C. E., Baltensperger, U., and Worsnop, D. R.: Evolution of organic aerosols in the atmosphere, *Science*, 326, 1525–1529, 2009.
- Johnson, D., Jenkin, M. E., Wirtz, K., and Martin-Reviejo, M.: Simulating the formation of secondary organic aerosol from photooxidation of aromatic hydrocarbons, *Environ. Chem.*, 2, 35–48, 2005.
- Jonsson, Å. M., Hallquist, M., and Saathoff, H.: Volatility of secondary organic aerosols from the ozone initiated oxidation of alpha-pinene and limonene, *J. Aerosol Sci.*, 38, 843–852, 2007.
- Jonsson, Å. M., Hallquist, M., and Ljungström, E.: The effect of temperature and water on secondary organic aerosol formation from ozonolysis of limonene,  $\Delta^3$ -carene and  $\alpha$ -pinene, *Atmos. Chem. Phys.*, 8, 6541–6549, doi:10.5194/acp-8-6541-2008, 2008.
- Kalberer, M., Paulsen, D., Sax, M., Steinbacher, M., Dommen, J., Prevot, A. S. H., Fisseha, R., Weingartner, E., Frankevich, V., Zenobi, R., and Baltensberger, U.: Identification of polymers as major components of atmospheric organic aerosols, *Science*, 303, 1659–1662, 2004.
- Kanakidou, M., Seinfeld, J. H., Pandis, S. N., Barnes, I., Dentener, F. J., Facchini, M. C., Van Dingenen, R., Ervens, B., Nenes, A., Nielsen, C. J., Swietlicki, E., Putaud, J. P., Balkanski, Y., Fuzzi, S., Horth, J., Moortgat, G. K., Winterhalter, R., Myhre, C. E. L., Tsigaridis, K., Vignati, E., Stephanou, E. G., and Wilson, J.: Organic aerosol and global climate modelling: a review, *Atmos. Chem. Phys.*, 5, 1053–1123, doi:10.5194/acp-5-1053-2005, 2005.
- Khovratovich, N. N., Novikova, T. M., Khmel'nitskii, A. I., Cherenkevich, S. N., and Loban, V. A.: IR spectra of preparations of ozonized pyrocatechin, *J. Appl. Spectrosc.*, 65, 201–205, 1998.
- Kroll, J. H. and Seinfeld, J. H.: Chemistry of secondary organic aerosol: Formation and evolution of low-volatility organics in the atmosphere, *Atmos. Environ.*, 42, 3593–3624, 2008.
- Kumagai, K., Iijima, A., Shimoda, M., Saitoh, Y., Kozawa, K., Hagino, H., and Sakamoto, K.: Determination of dicarboxylic acids and levoglucosan in fine particles in the Kanto Plain, Japan, for source apportionment of organic aerosols, *Aerosol Air Qual. Res.*, 10, 282–291, 2010.
- Kundu, S., Kawamura, K., Andreae, T. W., Hoffer, A., and Andreae, M. O.: Molecular distributions of dicarboxylic acids, ketocarboxylic acids and  $\alpha$ -dicarbonyls in biomass burning aerosols: implications for photochemical production and degradation in smoke layers, *Atmos. Chem. Phys.*, 10, 2209–2225, doi:10.5194/acp-10-2209-2010, 2010.
- Lay, T. H., Bozzelli, J. W., and Seinfeld, J. H.: Atmospheric photochemical oxidation of benzene: Benzene + OH and the benzene-OH adduct (Hydroxyl-2,4-cyclohexadienyl) + O<sub>2</sub>, *J. Phys. Chem.*, 100, 6543–6554, 1996.
- Lary, D. J., Shallcross, D. E., and Toumi, R.: Carbonaceous aerosols and their potential role in atmospheric chemistry, *J. Geophys. Res.*, 104, 15929–15940, 1999.
- Limbeck, A. and Puxbaum, H.: Organic acids in continental background aerosols, *Atmos. Environ.*, 33, 1847–1852, 1999.
- Mainelis, G., Willeke, K., Adhikari, A., Reponen, T., and Grinshpun, S. A.: Design and collection efficiency of a new electrostatic precipitator for bioaerosol collection, *Aerosol Sci. Tech.*, 36, 1073–1085, 2002.
- Moosmüller, H., Chakrabarty, R. K., Ehlers, K. M., and Arnott, W. P.: Absorption Ångström coefficient, brown carbon, and aerosols: basic concepts, bulk matter, and spherical particles, *Atmos. Chem. Phys. Discuss.*, 10, 24735–24761, doi:10.5194/acpd-10-24735-2010, 2010.
- Muckenhuber, H. and Grothe, H.: The heterogeneous reaction between soot and NO<sub>2</sub> at elevated temperature, *Carbon*, 44, 546–559, 2006.
- Mukai, H. and Ambe, Y.: Characterization of a humic acid-like brown substance in airborne particulate matter and tentative identification of its origin, *Atmos. Environ.*, 20, 813–819, 1986.
- Najera, J. J., Percival, C. J., and Horn, A. B.: Infrared spectroscopic studies of the heterogeneous reaction of ozone with dry maleic and fumaric acid aerosol particles, *Phys. Chem. Chem. Phys.*, 11, 9093–9103, 2009.
- Ng, N. L., Kroll, J. H., Chan, A. W. H., Chhabra, P. S., Flagan, R. C., and Seinfeld, J. H.: Secondary organic aerosol formation from *m*-xylene, toluene, and benzene, *Atmos. Chem. Phys.*, 7, 3909–3922, doi:10.5194/acp-7-3909-2007, 2007.
- Nieto-Gligorovski, L., Net, S., Gligorovski, S., Zetzsch, C., Jammoul, A., D'Anna, B., and George, C.: Interactions of ozone with organic surface films in the presence of simulated sunlight: impact on wettability of aerosols, *Phys. Chem. Chem. Phys.*, 10, 2964–2971, 2008.
- Nieto-Gligorovski, L., Net, S., Gligorovski, S., Wortham, H., Grothe, H., and Zetzsch, C.: Spectroscopic study of organic coatings on fine particles, exposed to ozone and simulated sunlight, *Atmos. Environ.*, 44, 5451–5459, doi:10.1016/j.atmosenv.2009.10.043, 2010.
- Nolting, W., Behnke, W., and Zetzsch, C.: A smog chamber for

- studies of the reactions of terpenes and alkanes with ozone and OH, *J. Atmos. Chem.*, 6, 47–59, 1988.
- Ofner, J., Krüger, H.-U., Zetzsch, C., and Grothe, H.: Direct deposition of aerosol particles on an ATR crystal for FTIR spectroscopy using an electrostatic precipitator, *Aerosol Sci. Tech.*, 43, 1–5, 2009.
- Ofner, J. and Grothe, H.: A mechanistic study of the cooperative effect of NO<sub>2</sub> and O<sub>2</sub> on the soot surfaces, *Asian Chem. Lett.*, 11, 57–61, 2007.
- Ofner, J., H.-U. Krüger, and Zetzsch, C.: Time resolved infrared spectroscopy of formation and processing of secondary organic aerosols, *Z. Phys. Chem.*, 224, 1171–1183, 2010.
- Olariu, R. I., Barnes, I., Becker, K. H., and Klotz, B.: Rate coefficients for the gas-phase reaction of OH radicals with selected dihydroxybenzenes and benzoquinones, *Int. J. Chem. Kinet.*, 32, 696–702, 2000.
- Polidori, A., Turpin, B. J., Davidson, C. I., Rodenburg, L. A., and Maimone, F.: Organic PM<sub>2.5</sub>: Fractionation by polarity, FTIR spectroscopy, and OM/OC ratio for the Pittsburgh aerosol, *Aerosol Sci. Tech.*, 42, 233–246, 2008.
- Pöschl, U., Martin, S. T., Sinha, B., Chen, Q., Gunthe, S. S., Huffman, J. A., Borrmann, S., Farmer, D. K., Garland, R. M., Helas, G., Jimenez, J. L., King, S. M., Manzi, A., Mikhailov, E., Pauliquevis, T., Petters, M. D., Prenni, A. J., Roldin, P., Rose, D., Schneider, J., Su, H., Zorn, S. R., Artaxo, P., and Andreae, M. O.: Rainforest aerosols as biogenic nuclei of clouds and precipitation in the Amazon, *Science*, 329, 1513–1516, 2010.
- Reinhardt, A., Emmenegger, C., Gerrits, B., Panse, C., Dommen, J., Baltensperger, U., Zenobi, R., Kalberer, M.: Ultra-high mass resolution and accurate mass measurements as new tools to characterize oligomers in secondary organic aerosol, *Anal. Chem.*, 79, 4074–4082, 2007.
- Salma, I., Mészáros, T., Maenhaut, W., Vass, E., and Majer, Z.: Chirality and the origin of atmospheric humic-like substances, *Atmos. Chem. Phys.*, 10, 131–1327, doi:10.5194/acp-10-1315-2010, 2010.
- Salma, I. and Láng, G. G.: How many carboxyl groups does an average molecule of humic-like substances contain?, *Atmos. Chem. Phys.*, 8, 5997–6002, doi:10.5194/acp-8-5997-2008, 2008.
- Samburova, V., Didenko, T., Kunenkov, E., Emmenegger, C., Zenobi, R., and Kalberer, M.: Functional group analysis of high-molecular weight compounds in the water-soluble fraction of organic aerosols, *Atmos. Environ.*, 41, 4703–4710, 2007.
- Sax, M., Zenobi, R., Baltensperger, U., and Kalberer, M.: Time resolved infrared spectroscopic analysis of aerosol formed by photo-oxidation of 1,3,5-trimethylbenzene and  $\alpha$ -pinene, *Aerosol Sci. Tech.*, 39, 822–830, 2005.
- Schmitt-Kopplin, Ph., Gelencsér, A., Dabek-Zlotorzynska, E., Kiss, G., Hertkorn, N., Harir, M., Hong, Y., and Gebefügi, I.: Analysis of the unresolved organic fraction in atmospheric aerosols with ultrahigh-resolution mass spectrometry and nuclear magnetic resonance spectroscopy: Organosulfates as photochemical smog constituents, *Anal. Chem.*, 82, 8017–8026, 2010.
- Shapiro, E. L., Szprengiel, J., Sareen, N., Jen, C. N., Giordano, M. R., and McNeill, V. F.: Light-absorbing secondary organic material formed by glyoxal in aqueous aerosol mimics, *Atmos. Chem. Phys.*, 9, 2289–2300, doi:10.5194/acp-9-2289-2009, 2009.
- Socrates G.: Infrared characteristic group frequencies, John Wiley and Sons, Wiley, New York, 1980.
- Sonntag, D.: Important new values of the physical constants of 1986, vapor pressure formulations based on the ITS-90 and psychrometer formulae, *Z Meteorol.*, 70, 340–344, 1990.
- Stevenson, F. J.: Humus chemistry: genesis, composition and reactions, 2nd ed.; Wiley, New York, 1994.
- Stevenson, F. J. and Goh, K. M.: Infrared spectra of humic acids and related substances, *Geochim. Cosmochim. Ac.*, 35, 471–483, 1971.
- Stone, E. A., Hedman, C. J., Sheesley, R. J., Shafer, M. M., and Schauer, J.: Investigating the chemical nature of humic-like substances (HULIS) in North American atmospheric aerosols by liquid chromatography tandem mass spectrometry, *Atmos. Environ.*, 43, 4205–4213, 2009.
- Sun, Y. L., Zhang, Q., Anastasio, C., and Sun, J.: Insights into secondary organic aerosol formed via aqueous-phase reactions of phenolic compounds based on high resolution mass spectrometry, *Atmos. Chem. Phys.*, 10, 4809–4822, doi:10.5194/acp-10-4809-2010, 2010.
- Tomas, A., Olariu, R. I., Barnes, I., and Becker, K. H.: Kinetics of the reaction of O<sub>3</sub> with selected benzenediols, *Int. J. Chem. Kinet.*, 35, 223–230, 2003.
- Vesna, O., Sax, M., Kalberer, M., Gaschen, A., and Ammann, M.: Product study of oleic acid ozonolysis as function of humidity, *Atmos. Environ.*, 43, 3662–3669, 2009.
- Yu, Y., Ezell, M. J., Zelenyuk, A., Imre, D., Alexander, L., Ortega, J., D’Anna, B., Harmon, C. W., Johnson, S. N., and Finlayson-Pitts, B. J.: Photooxidation of alpha-pinene at high relative humidity in the presence of increasing concentrations of NO<sub>x</sub>, *Atmos. Environ.*, 42, 5044–5060, 2008.
- Zellner, R., Behr, P., Seisel, S., Somnitz, H., and Treuel, L.: Chemistry and microphysics of atmospheric aerosol surfaces: Laboratory techniques and applications, *Z. Phys. Chem.*, 223, 359–385, 2009.